Flow Velocity Profile via Time-Domain Correlation: Error Analysis and Computer Simulation

STEVEN G. FOSTER, PAUL M. EMBREE, MEMBER, IEEE, AND
WILLIAM D. O'BRIEN, JR., FELLOW, IEEE

Abstract—**An ultrasonic flow velocity profile measurement method employing time-domain correlation of consecutive echo pairs has been developed. The time shift between a pair of range gated echoes is estimated by searching for the shift that results in the maximum correlation. This technique is fundamentally different than the autocorrelation techniques that do not search for the maximum correlation. The time shift indicates the distance a group of scatterers has moved from which flow velocity is estimated. The basis for the computer simulations and error analyses of the scheme includes a band passed white Gaussian noise signal model for an echo from a scattering medium, the estimate of flow velocity from both a single scatterer and multiple scatterers, and a derived precision estimation. The error analysis via computer simulation includes an evaluation of errors associated with the correlation method. For a uniform flow velocity profile, beamwidth modulation represents the greatest error source. However, for a nonuniform flow velocity profile, the jitter caused by a small flow velocity gradient can exceed the other error sources. A detailed computer simulation evaluated the interdependencies of window length, beamwidth, vessel diameter and viewing angle on the estimation of flow velocity. One-dimensional (1-D) flow velocity profiles across the vessel can be obtained but there are engineering trade-offs of beamwidth and window length with the physiologic flow velocity gradient across the range cell to achieve the desired precision. The analyses reported herein are specific for the case when the measured component of flow velocity is parallel to the ultrasound beam axis, that is, axial flow velocity.**

I. Introduction

THE measurement of human blood flow velocity by ultrasonic techniques has proved to be a valuable tool for clinical diagnosis of vascular disease. Unfortunately, current Doppler based measurement techniques are plagued with practical as well as theoretical difficulties that result in inaccurate and imprecise flow velocity estimates [1], [2]. Doppler blood flow velocity measurement techniques have been well researched from a theoretical [3]–[5] as well as a practical [6]–[12] point of view. The Doppler frequency shift of high frequency ultrasound, while rather easy to detect, is difficult to assess with useful accuracy [1], [2]. While most investigators have studied the Doppler techniques that were originally used in radar systems [13], we have chosen to use time-domain correlation techniques.

This paper introduces a method to measure the axial flow velocity in an optimum way by the time-domain correlation technique. The axial flow velocity is the component of the flow velocity in the direction of the ultrasonic beam axis. The flow velocity can be calculated from the axial flow velocity measurement if the angle between the beam axis and the direction of flow (measurement angle) is known. In this paper, the foundation of this scheme is developed and verified through computer simulation. In the companion paper [14] the technique is verified through experimental techniques and compared to a quantitative volumetric standard for continuous flow.

Other investigators [15]–[19] have suggested using time-domain correlation to measure flow velocity. This work, although unknown to us during the time the research was being conducted, suggests an almost identical formulation of a flow velocity measurement method by time-domain correlation. In our work we have attempted to be more complete in the error analysis and accuracy verification.

The time-domain correlation technique can be conceptually viewed in the following way for a point scatterer: At time $t = t_0$ a scatterer is located at position X, and at time $t = t_0 + T$ that scatterer has moved to a new position Y. Hence, the speed is $(Y - X)/T$, where T is the time difference between the transmission of two (not necessarily consecutive) pulses. The two echoes are amplified and digitized using a high speed analog to digital converter (A/D) for computer processing. Part of the first echo is windowed and shifted over the second echo to locate where the windowed data most closely matches the second echo. The degree of similarity is assessed from the correlation of the windowed section of the two echoes. The amount that the two data sets are shifted in order to obtain the maximum correlation is directly related to the axial velocity of the scatterers from the transducer.

To evaluate the time-domain correlation technique, the signal model for an echo from a scattering medium will be presented. This model is the basis for all subsequent computer simulations. The flow velocity will then be de-

Manuscript received August 3, 1988; revised December 15, 1989; accepted December 20, 1989. This work was supported in part by the American Heart Association, Illinois Affiliate, the National Institutes of Health, National Cancer Institute, CA 09067, and in part by the National Institutes of Health, National Institute of Heart, Blood and Lung Institute, HL 39704.

S. G. Foster is with Nicolet, P.O. Box 7010, 20001 South Stoughton Road, Madison, WI 53716.

P. M. Embree is with Philips Ultrasound, 2722 South Fairview Street, Santa Ana, CA 92704.

W. D. O'Brien is with the Bioacoustics Research Lab, Department of Electrical and Computer Engineering, University of Illinois, 1406 West Green Street, Urbana, IL 61801.

IEEE Log Number 9034358.

termined from the time-domain correlation technique for both a single scatterer and multiple scatterers. In this section, the theoretical precision of the time-domain correlation technique will also be evaluated.

A. Signal Model of an Echo from a Scattering Medium

The signal model for an ultrasonic echo from a scattering medium with a large number of scatterers per wavelength (such as blood) is modeled as band passed white Gaussian noise (BPWGN). Based upon Angelsen's model [20] where there are a large number of scatterers in a small volume, the reflection coefficient of each particle can be modeled approximately as a Gaussian independent variable. Therefore, the ultrasonic echoes are assumed to be independent and Gaussian distributed. The received signal is considered to be bandlimited since the exciting ultrasonic pulse is bandlimited. There is also some bandlimiting due to the frequency response of the receive amplifier and the nonzero size of the scatterer, although these effects are small compared to the band-limiting of the transducer.

The signal at the receiving transducer consists of the sum of all the individual echoes from each of the acoustic particles, delayed by the round-trip time between the transducer and particle. The mathematical representation of the received electrical signal is given by

$$w(t) = \int_V A(\bar{R}) h\left(\bar{R}, t - \frac{2|\bar{R}|}{c}\right) dV \qquad (1)$$

where $A(\bar{R})$ is the random reflection coefficient (zero mean, variance σ^2), $h(\bar{R}, t - 2|\bar{R}/c)$ is the system impulse response and c is the speed of sound in the medium. The system impulse response represents the echo from the particle dV positioned at $\bar{R}$ with a reflection coefficient of unity. Since the system is assumed to be linear and bandlimited, it is characterized by a position dependent ultrasonic impulse response.

B. Velocity Determination: Single Scatterer

The essence of the time-domain flow measurement technique, schematically shown in Fig. 1, is to track scatterers in a range cell within an ultrasonic beam and assess the distance traveled by the time shift between echoes. The change in range (from position 1 to 2 in Fig. 1) of a single scatterer's echo is found by a correlation procedure. The range of the first echo waveform, $w_1(t)$, results from an ultrasonic pulse transmitted at $t = t_0$. At a later time $t_0 + T$, a second ultrasonic pulse is transmitted and the second echo waveform, $w_2(t)$, is received, but shifted in time by $t_s + T$ from the first echo. In effect, the time-axis origin is reset since the T term is ignored. The second echo is shifted by t_s from the first. This approach is carried-out throughout the paper.

The correlation function of the two echoes is defined by

$$R(\tau) = \int_{-\infty}^{\infty} w_1(t) w_2(t + \tau)\ dt. \qquad (2)$$

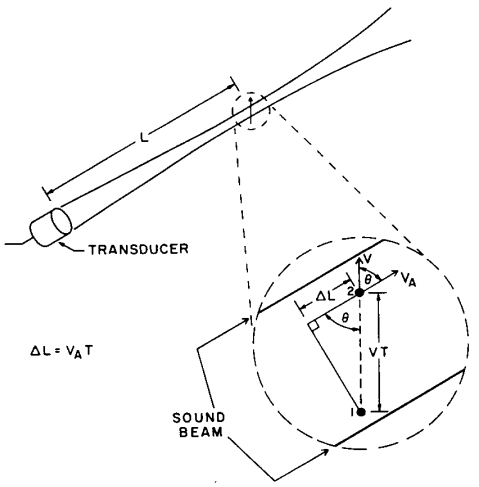

Fig. 1. Schematic representation of sound beam relative to the direction of flow of scatterers. Here, the initial position 1 of scatterer is shifted distance VT to position 2. Angle θ is measurement (Doppler) angle and L is range from transducer.

The two echoes are identical except for the second echo being time delayed from the first, and expressed as

$$w_2(t) = w_1(t - t_s). \qquad (3)$$

Hence,

$$R(\tau) = \int_{-\infty}^{+\infty} w_1(t) w_1(t - t_s + \tau)\, dt = R_{11}(\tau - t_s) \qquad (4)$$

where $R_{11}(\tau - t_s)$ is the autocorrelation function of $w_1(t)$ and maximal when the argument of the autocorrelation function is zero, i.e., when $\tau = t_s$. The magnitude of change in range of the second echo with respect to that of the first echo is found at the position where the correlation function of the two echoes is maximal.

In Fig. 1, the axial component of the scatterer's velocity along the beam axis is V_A. The axial distance that the scatterer has moved in time T is designated as ΔL where $\Delta L = V_A T = VT \cos(\theta)$. At time $t = t_0$ an ultrasonic pulse is transmitted, and at time $t = t_0 + t_1$ the echo from the scatterer at position 1 is received. At time $t = t_0 + T$ a second pulse is transmitted and the echo from the scatterer at position 2 arrives at time $t = t_0 + T + t_2$. The propagation time for the echo from position 2 is $t_2 - t_1$ greater than that for the echo returned from position 1. This is the time shift between the two echoes from this one scatterer, that is, $t_s = t_2 - t_1$, where t_S is positive when the scatterer is moving away from the transducer (as in Fig. 1) and negative when the scatterer is moving towards the transducer. The axial flow velocity component is (assuming $V_A \cos(\theta) \ll c$)

$$V_A = \frac{c(t_2 - t_1)}{2T} = \frac{ct_s}{2T}. \qquad (5)$$

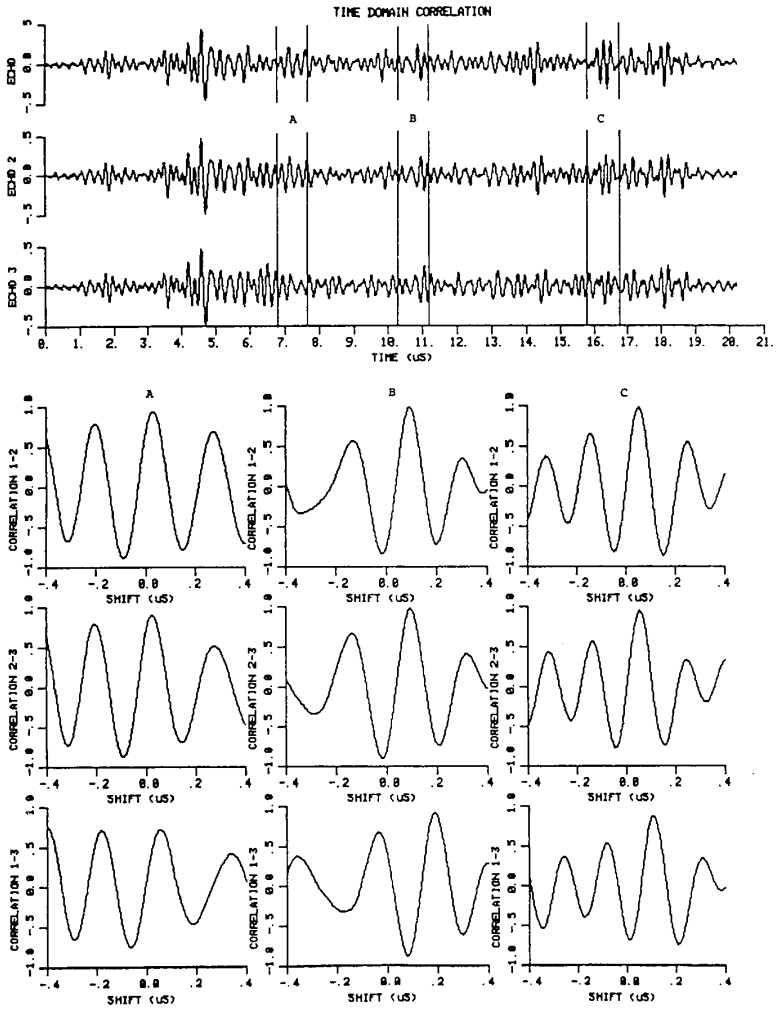

Fig. 2. Time-domain correlation method example for typical experimental data for $\theta = 45°$. Upper three plots show three consecutive echoes sampled at 50-MHz sampling rate with $T = 384$ μs. Lower nine plots show correlation coefficients versus shift for three 0.8 μs range gates (A, B, and C).

Since the vessel is orientated at an angle θ (the measurement angle) the result must be scaled by $1/\cos(\theta)$, to yield the speed of the scatterer as (assuming $V \cos(\theta) \ll c$)

$$V = \frac{ct_s}{2T \cos(\theta)}. \tag{6}$$

C. Velocity Determination: Multiple Scatterers

To determine the shift between echoes at a particular range for multiple scatterers, a rectangular window is used to remove a range cell from the first signal at the desired range. This range cell is overlaid onto the second signal until the maximum correlation is located. The shift with the maximum correlation is taken to be the true shift. For the special case where there is no noise, all particles have the same velocity and the complete echo is contained within the range cell, the point of maximum correlation is the same as the true shift, since the correlation is the autocorrelation function of the echo. The shift $\hat{\tau}$ where maximum correlation occurs is determined by

$$\hat{\tau} = \max_{\tau} \int_a^b w_1(t) w_2(t + \tau)\, dt \tag{7}$$

where $w_1(t)$ and $w_2(t + \tau)$ represent the windowed segments of their respective waveforms and max means the value of τ for which the integral is maximum. The shift $\hat{\tau}$ in (7) is similar to that of t_s for the single scatterer case in (6).

Fig. 2 shows three consecutive ultrasonic signals obtained using a 5-MHz transducer directed at a 6-mm diameter dialysis tube containing a flowing water and Seph-

adex® mixture, used as a blood mimicking substance. The experimental set-up is described in [14]. The front wall signal is near 4.5 μs and the back wall echo is near 18 μs. The center sections of the signals appear to move to the right slightly while sections near the walls do not move.

Three 0.8-μs range-gated sections of the three signals are denoted by the symbols A, B, and C in the upper curves of Fig. 2. These are used to illustrate the time-domain correlation method in the figure's lower portion. The discrete time correlation coefficient between two rectangularly windowed, zero mean signal sections, $e_1(n)$ and $e_2(n)$ is given by

$$\rho(s) = \frac{\sum_{i=0}^{N-1} e_1(r+i)e_2(r+i+s)}{\sqrt{\sum_{j=0}^{N-1}\left[e_1(r+j)\right]^2 \sum_{k=0}^{N-1}\left[e_2(r+k+s)\right]^2}} \tag{8}$$

where s is the shift between signals (samples), r is the range to beginning of section to be measured (samples), $\rho(s)$ is the correlation coefficient between echoes ($-1 \leq \rho(s) \leq 1$), and N is the window length (samples). For the sample correlation functions shown in Fig. 2, the window length was 40 samples and the sampling rate (f_s) was 50 MHz so that 40 samples correspond to a round-trip length of 4 λ at 5 MHz. The physical length of the cell is one-half this value, that is, 2 λ, since range is determined by round-trip travel time (here 0.8 μs) and the "range cell length" is therefore $cN/2f_s$ or 0.62 mm (for c = 1540 m/s). Previous work [21], [22] indicated that this window length is a good compromise between range resolution and measurement precision (as discussed in Section III-B of this paper).

The three columns of correlation coefficient functions in Fig. 2 represent correlations at ranges A, B, and C. The top row represents correlations of signal 1 with signal 2, the middle row of signal 2 with signal 3 and the bottom row of signal 1 with signal 3. As the examples show, the maximum correlation of the center section (range B) is a positive time shift, corresponding to a flow velocity away from the transducer. The correlation peak of signal 1 with signal 3 is at a shift twice that of signal 1 with signal 2 or signal 2 with signal 3. The two correlation examples near the tube walls (ranges A and C) show less shift, as expected for the case of fully developed laminar flow.

Because the signal is sampled at discrete times, the correlation function can be calculated only at discrete time delays and the maximum is likely to fall between two points, limiting the accuracy of the location of the correlation peak. The method used to estimate the maximum point of the correlation function is to find the maximum discrete correlation and its two neighboring points, fit a parabola to the points, and determine the maximum of the parabola [22], [23]. This is illustrated in Fig. 3. A computer evaluation of the variance of this estimate (jitter) versus samples per wavelength (or sampling rate/center frequency) is shown graphically in Fig. 4 for 3 system Q's (ratio of the center frequency of the ultrasonic pulse to its 3-dB bandwidth), and it is quite small (for ten samples per wavelength) when compared to the precision of the time domain correlation method [22].

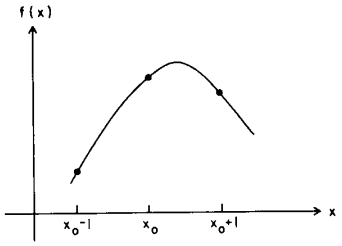

Fig. 3. Graphical representation that shows that three points of correlation function near its maximum can be approximated by parabola.

The magnitude of the velocity of the scatterer at a particular range is given by

$$V = \frac{s_{\max} c}{2T \cos(\theta)} \tag{9}$$

where $s_{\max}$ is the time shift with maximum correlation.

Since the time-domain correlation method compares two successive echoes that have passed through the same intervening tissue, frequency dependent attenuation of the tissue path will not affect the mean flow velocity measurement. Thus, the average time shift determined by time domain correlation is unbiased by the frequency response of the tissue.

II. Error Analysis

A. Precision of Time-Domain Correlation Method

The derivation of the precision of the time-domain method is essentially identical to the derivation of the time arrival of a radar signal [24], [25]. The derivation's overall assumption is the signal level is large compared to the noise level. The derivation also assumes that the window length is large compared to the ultrasound wavelength and the correlation peak can be estimated from a wideband signal with additive white noise [21]. The validity of these assumptions is addressed later (see Section III).

It is also assumed that the additive white noise present in the two received signals causes a small deviation (much less than a wavelength) in the time-delay estimate ($\hat{\tau}$). Here the noise is small compared to echoes and the echoes are highly correlated at the true time delay (τ_0). Thus, the variance of $\hat{\tau}$ about τ_0 is [21]

$$\mathrm{VAR}\left[\hat{\tau}\right] = \frac{2N_0}{\beta^2 \rho^2 E} \tag{10}$$

where N_0 is the white noise power spectral density of each echo (W/Hz), β is the RMS bandwidth of the received

®Sephadex is a registered trademark of Pharmacia Fine Chemicals, Uppsala, Sweden.

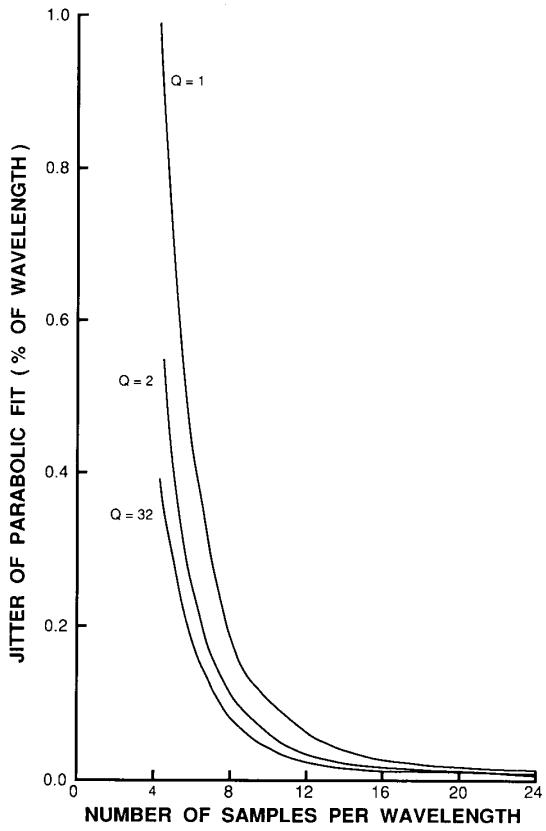

Fig. 4. Graphical representation of jitter (variance of this estimate) resulting from the parabolic fit as function of number of samples per wavelength for three system Q's.

echoes (rad/s), ρ is the maximum correlation coefficient of the echoes without noise and E is the average energy of each range gated echo (J). Thus, the precision of the time-domain correlation velocity estimate $[\sqrt{\text{VAR}(\hat{\tau})}/\tau_0]$ is

$$\text{Precision}\,[\hat{\tau}] = \frac{\sqrt{2}}{\beta\rho\tau_0\,\text{SNR}} \tag{11}$$

where SNR is the signal-to-noise ratio, $\sqrt{E/N_0}$. For a sampled signal where the noise spectral density is constant with frequency, the SNR is given by $\sqrt{N\,\text{VAR}(s)/\text{VAR}(n)}$, where N is the number of samples in the range gate, VAR (s) is the signal variance and VAR (n) is the noise variance in the range gate.

As indicated by (11), the precision of the time shift estimate is inversely related to the product of the SNR and RMS bandwidth. The precision value for each time shift improves by an order of magnitude when the SNR is increased from 10 dB to 30 dB. The precision of the time shift estimate can be improved by decreasing the pulse repetition frequency that would result in a larger mean time shift for the same axial flow velocity. However, as more scatterers enter and leave the beam during the time between echoes, the maximum correlation of the consecutive echoes decreases. Thus, the precision of the velocity estimate will decrease as the time between echoes increases. On the other hand, if the time between echoes decreases to a very small value, the point of maximum correlation and the corresponding velocity estimate will vary randomly due to the random noise in the backscattered signal.

Fig. 5 shows an experimental result of the correlation coefficient as a function of lateral separation distance. From these measurements and the theoretical result for a cylindrical beam [22], a nearly linear approximation (assuming the correlation function is independent of θ) appears valid. When the lateral separation distance is one-half of the beamwidth, the correlation coefficient is reduced from 1.0 to about 0.4. The linear curve in Fig. 5 can be expressed as

$$\rho(a) = 1 - 1.2a \tag{12}$$

where a is the fraction of the beamwidth the scatterers have moved perpendicular to the beam (lateral separation) and is represented in terms of the scatterers' velocity, V, time between initiation of the transmitted pulses, T, the 3-dB beamwidth, BW, at the measurement range and the measurement angle, θ, as

$$a = \frac{VT\sin(\theta)}{BW}, \tag{13}$$

and is valid over the approximate range $0 < a < 0.6$ as estimated from Fig. 6. Because the highly focused transducer beamwidth is only 2.3 wavelengths ($F = 2$) and the window length is only 4 λ (round trip), the small velocity gradient at the center of the parabolic profile should not affect this measurement.

Fig. 6 shows the precision (see (11)) of the time shift estimate for different transducer measurement angles and the linear correlation coefficient function of (12). These values were typical for the experimental measurements with the 5-MHz transducer used in flow measurements with an SNR of 20 dB [14], [21]. For each measurement angle, the precision value decreases to a minimum value (3.7% at 482 ns for 30°; 6.5% at 278 ns for 45°; 11.2% at 160 ns for 60° and 24.2% at 74 ns for 75°) and then begins to increase due to the decorrelation of the echoes.

In summary, the theoretical precision of the time-domain correlation method depends on the measurement angle, the system RMS bandwidth, the mean time shift between echoes, and the SNR.

B. Errors Associated with Correlation Method

In this discussion the term "range cell" is defined as the volume of scatterers contained within the windowed segment of the echo. Since the echoes from the scattering medium cannot be entirely contained in the correlation window, there are several sources of error associated with the correlation method. They are: 1) a windowed waveform does not necessarily have its maximum correlation at the true shift; 2) the range cell contains scatterers that

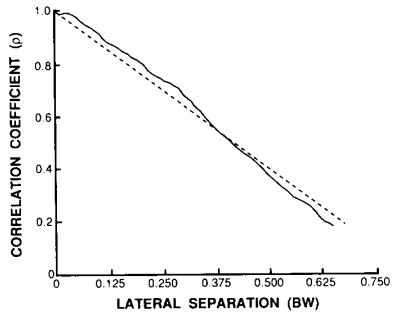

Fig. 5. Measured correlation coefficient (solid line) and its linear approximation (dashed line) versus lateral separation distance (expressed as fraction of beamwidth perpendicular to beam axis). Measurement was made at the center of 23-λ diameter tube in which constant laminar flow was established. 5 MHz, highly focused transducer ($F = 2$) beamwidth was 2.3 λ, correlation length was 4 λ, and measurement angle (θ) was 45°.

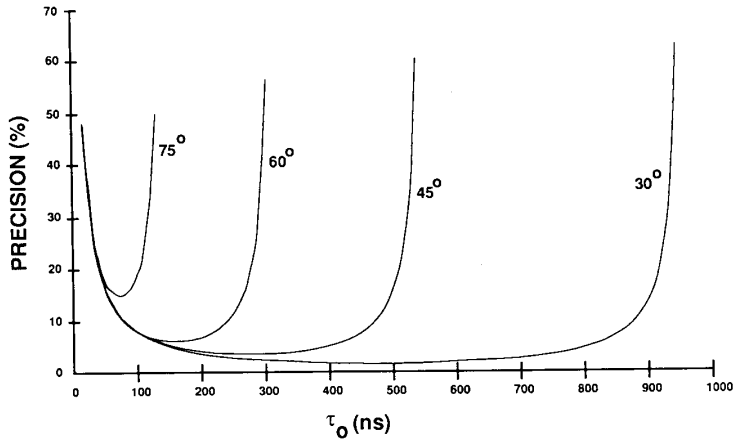

Fig. 6. Theoretical precision ((11)) versus time shift and measurement angle. Beam decorrelation is assumed to be linear. SNR is 20 dB (10), RMS bandwidth is 2.5 MHz (15.7 Mr/s) and beamwidth is 0.6 mm.

move at different velocities; 3) an actual range cell will contain ultrasonic energy from scatterers outside the range cell due to finite bandwidth effects; and 4) as the scatterer moves through the beam, the backscattered ultrasonic signal is modulated by the field pattern of the transducer.

1) Error Associated with Windowing: The process of windowing may shift the point of maximum correlation away from the true shift if the echoes are identical. To evaluate this error sources, the second echo will be assumed to be identical to the first with no shift. Hence the true shift between the two echoes must be zero. The estimated shift, $\hat{\tau}$, is defined by (7). A computer simulation has been used to determine the bias and variance of the estimate $\hat{\tau}$ and showed that $\hat{\tau}$ was unbiased (zero mean) for all rectangular correlation windows [22].

The term "jitter" in Fig. 7 is defined as the standard deviation (square root of the variance) of the estimate $\hat{\tau}$. The signal model used in the simulation is band-passed white Gaussian noise (BPWGN) and the system Q is defined to be the ratio of the center frequency of the ultrasonic pulse to its 3 dB bandwidth. A six-pole Chebyshev response is used (with 1-dB ripple) in order to simulate the transfer function of the transducer and receiver electronics. The window length is shown in wavelengths of the center frequency of the ultrasonic pulse.

The jitter decreases as the window length increases because the correlation more closely approximates the autocorrelation function (which has zero jitter in estimating of the true shift). The bottom curve of Fig. 7 simulates a BPWGN with an infinite Q (purely sinusoidal). Note that the minima and maxima occur in the same positions for a Q of 32 as those of the infinite BPWGN case. This is expected since, with a Q of 32, waveform will closely resemble a slowly modulated sinusoid. As the value of Q decreases further the minima and maxima lose their identity as compared to those of a higher Q system. Fig. 8 shows the jitter versus Q for various correlation lengths where the correlation lengths were chosen as the worst

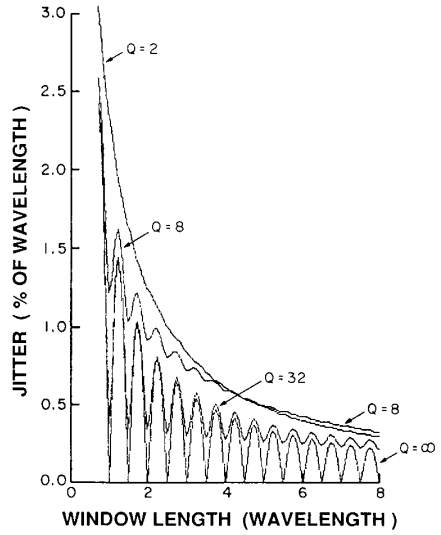

Fig. 7. Graphical representation of jitter (standard deviation of estimate $\hat{\tau}$) as function of window length for four system Q's.

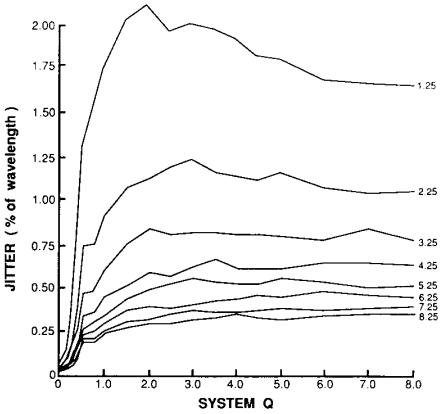

Fig. 8. Graphical representation of jitter as function of system Q for eight different window lengths. From top-to-bottom the window lengths are 1.25, 2.25, 3.25, 4.25, 5.25, 6.25, 7.25, and 8.25 λ.

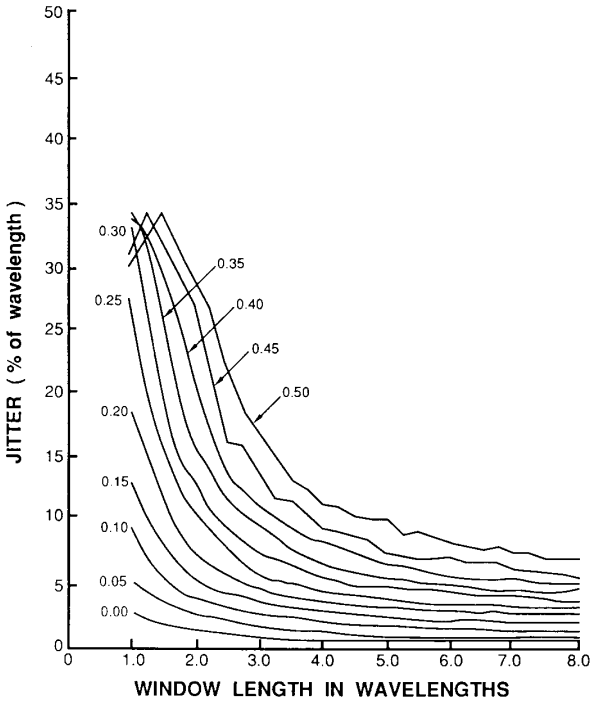

Fig. 9. Graphical representation of jitter (standard deviation of the estimate $\hat{\tau}$) as function of window length of eleven scatterer separation distances (in wavelengths) for a system Q of 2.

case lengths for the pure sinusoid case (n + 0.25 wavelengths where n is an integer).

2) Error Associated with Scatterers Moving at Different Velocities Within the Range Cell: The scatterers within a range cell will be moving at different velocities since the velocity profile across the vessel is not necessarily uniform. Thus, only part of the range cell of the first signal will line up with the corresponding part of the second signal. The other parts of the signal of the first echo will not be perfectly aligned with their corresponding parts in the second echo since these parts come from scatterers that are moving with different velocity. A computer simulation was used to estimate the jitter due to different flow rates in the range cell and the results are graphically represented in Fig. 9 where jitter is plotted as a function of window length for various scatterer separation distances.

Separation is defined (in wavelengths) as the distance that the fastest scatterer gains over the slowest scatterer in the time interval between the initiation of successive echoes [22]. The separation is a one-way separation. For this simulation, the scatterers at the edge of the range cell nearest to the transducer are assumed to have the slowest velocity and the scatterers at the farthest edge are assumed to have the fastest velocity. The scatterers between these two edges are assumed to have velocities that increase linearly with depth into the range cell.

Because of the results shown in Figs. 7 and 8, the characteristics shown in Fig. 9 should be similar for other system Q's (here Q = 2). The effect of the finite correlation window length is shown in the bottom curve (zero separation); if the correlation window effect were not present, then this curve would lie on the horizontal axis. Separation can be determined analytically for fully developed laminar flow from the axial velocity profile, $V_\lambda(r)$,

$$V_\lambda(r) = V_{\max}\left[1 - (2r/N_\lambda)^2\right] \qquad (13)$$

where $V_{\max}$ is the maximum axial velocity in wavelengths per unit time, r is the axial distance variable in wavelengths and N_λ is the vessel diameter in wavelengths (see Fig. 10). The change in distance, $S(r)$, experienced by the scatterers at the end of the range cell compared to those at the beginning of the range cell in time, T, the time

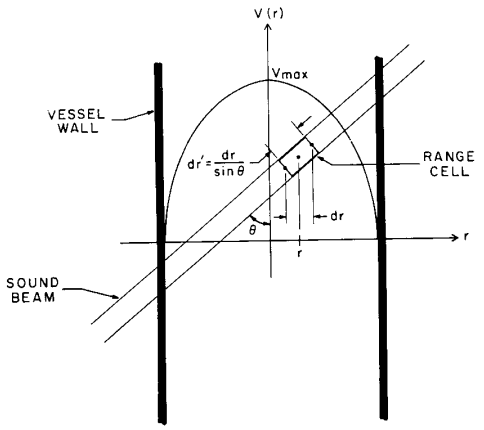

Fig. 10. Geometry used in derivation of jitter resulting from error associated with scatterers moving at different velocities within range cell.

interval between the initiation of the pulses is approximately

$$S(r) = T\left[V_\lambda(r + dr/2) - V_\lambda(r - dr/2)\right] \quad (14a)$$

$$= T\frac{d}{dr}V\lambda(r)\,dr = -4(TV_{\max}/N\lambda)(2r/N\lambda)\,dr \quad (14b)$$

where dr is the range cell length projected on r-axis in wavelengths. The worst-case separation occurs at the vessel walls, where

$$S(N_\lambda/2) = -4\frac{TV_{\max}}{N_\lambda}\,dr. \quad (15)$$

Equation (14b) can be formulated in terms of experimentally measured quantities. The distance that a midstream scatterer moves in time T is $TV_{\max}$. However, the system measures directly the increase in round-trip path length due to this movement, that is, $s = 2TV_{\max}\cos\theta$, where s is defined as this axial separation distance. The value dr can be related to the range cell axial length, dr' (determined by the window length) where $dr = dr'\sin\theta$. Therefore,

$$S(r) = -2(s/N_\lambda)(2r/N_\lambda)\tan\theta\,dr'. \quad (16)$$

For a 6.96 mm diameter vessel ($N_\lambda = 24\ \lambda$) inclined at 45° with respect to the transducer, an ultrasonic pulse with a center frequency of 5 MHz, Q at 4, a measured s of 0.7 λ, and a window length (dr') of 8 λ (physical length of range cell is 4 λ because of round-trip time) the calculated worst-case separation (at vessel wall, that is, at $r = 12\ \lambda$) would be 0.47 λ. The jitter associated with the velocity estimate using an 8 λ window length is about 6% of a wavelength (from Fig. 9). Normalizing the jitter by the axial velocity (i.e., dividing the jitter by the axial flow, $s = 0.7$) yields a value of 8%.

This is roughly the amount of normalized jitter found experimentally for this size vessel with this amount of s for a window length of 6.5 λ. The range cell will be slightly larger than a 6.5 λ window length because the Q is not zero. The cell will be roughly 1.5 λ longer due to the Q, bringing the total window length to 8 λ, which is what was used previously. The error becomes smaller as the range cell nears the center of the vessel.

3) Error Associated with Time Duration of the System Impulse Response: The system impulse response is the waveform at the output of the system due to the ultrasonic pulse (generated and detected by the system) reflecting from a single scatterer. The echo from a medium which consists of many scatterers is the convolution of the system impulse response with the density function of the scatterers. The bandlimited frequency response of the system will cause the received signal at a particular range to be the result of the convolution of the system impulse response with the energy reflecting from scatterers. The longer the temporal duration of the impulse response, the greater will be the fraction of energy at a particular range arising from energy from earlier scatterers in the range cell (and before the range cell). The velocity estimate will be shifted towards the velocities of those earlier scatterers. In addition to the velocity estimation being biased towards early scatterers, the estimate will also lose range resolution. The mathematical representation of this effect is assumed to be

$$\hat{V}(\tau) = \frac{\int_{-\infty}^{\tau} V(t)\left|h(\tau - t)\right|^2 dt}{\int_{0}^{\infty}\left|h(t)\right|^2 dt} \quad (17)$$

where τ represents the location of range cell, $V(t)$ is the velocity profile that the pulse passes through, $h(t)$ is the system impulse response (assumed causal), and $\hat{V}(\tau)$ is the estimate of velocity at range. For good range resolution, $h(t)$ must have the lowest possible temporal duration.

4) Error Associated with Intensity Profile Across the Sound Beam: As a scatterer passes through a sound beam the intensity of the scattered ultrasound will be directly proportional to the intensity of the sound beam at the scatterer location. Hence, the intensity of a scatterer will increase as the scatterer nears the axis of the beam and will decrease as the scatterer moves away from the axis. This amplitude modulation effect is known as beamwidth modulation. With many scatterers in the beam, some will be approaching the beam axis and some will be moving away from the beam axis, causing two successive echoes to look less similar. The jitter of the estimate $\hat{\tau}$ due to this error source is shown in Fig. 11. Here jitter (standard deviation expressed as a percentage of the wavelength) is presented as a function of the fractional amount of beamwidth that the scatterer moves for various window lengths. The lat-

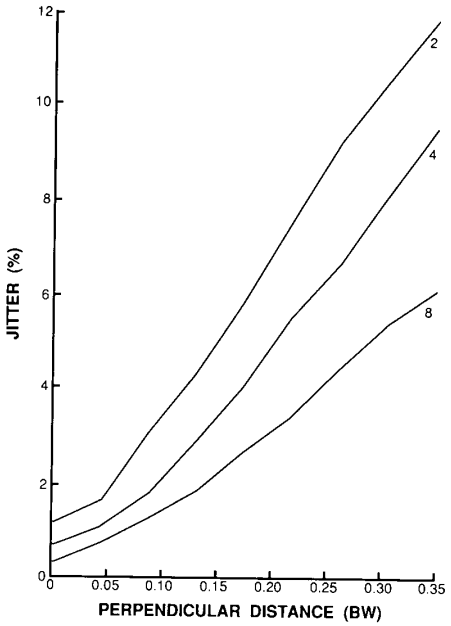

Fig. 11. Graphical representation of beamwidth modulation jitter (standard deviation of the estimate $\hat{\tau}$) as function of distance the scatterer moves across the beamwidth (normalized to the 3 dB beamwidth) for three window lengths of 2, 4, and 8 λ with system Q of 2.

eral distribution of the sound beam is assumed to have a Gaussian profile. For the case of no scatterer movement, the jitter reduces to the jitter associated with the window length effect (see Fig. 9). The error associated with the beam profile dwarfs the correlation effect for good SNR.

In summary, the error from the beamwidth modulation of the scatterers represents the greatest source of error for velocity estimation where all of the scatterers in the beam are moving at the same velocity. When the scatterers within the range cell are moving at different velocities, the jitter caused by a small velocity gradient can easily exceed the other error sources.

IV. Verification by Computer Simulation

A detailed computer simulation was performed in order to evaluate the effects of the system quantities on the estimation of flow velocity at various points across a vessel [22]. Within the beamwidth the intensity is nonzero; outside the beamwidth no sound is assumed to exist. No noise was added to the simulation and no averaging of velocity results was performed. All distance measurements are in wavelengths relative to the center frequency of the ultrasonic pulse.

Fig. 12(a) shows one example of the computer simulation results of the velocity profiles determined by the time-domain correlation method. The topmost curve is the actual parabolic velocity profile that an unbiased ultrasonic flow meter would measure. The other top curve is the time-domain correlation method estimate of the velocity profile. Both velocity profile curves are normalized to the midstream value of the actual velocity with the maximum of the actual flow at 100%. The standard deviation curve is the jitter of the estimate normalized by dividing by the maximum actual axial flow. The precision curve (in percent) is a measure of the precision of the velocity estimation algorithm and consists of the jitter (standard deviation of the velocity estimate) divided by the estimate of the mean velocity expressed as a percentage. The precision curve is not normalized. When the value exceeds 100%, it is truncated to 100%. The same graphical format is used in Figs. 12(b), (c), and (d) for which the respective vessel diameter are 24, 12, and 6 λ (four different measurement angles are shown in each of Figs. 12(b), 12(c), and 12(d).

The standard deviation curves of Figs. 12(b)–(d) indicate the total jitter from all sources discussed in Section III-B. The primary jitter errors are from beamwidth modulation and from velocity gradients across the range cell. Since these three figures have the same size range cell, the velocity gradient across the range cell should be smallest in the largest vessel. The contribution to midstream jitter from velocity gradients is least in the largest vessel (24 λ) at the smallest viewing angle (45°). A smaller viewing angle will result in a longer path through the vessel minimizing further the effect of velocity gradients. In Fig. 12(b) (upper right) the midstream jitter is 3.7%.

The perpendicular positional change ($s_\perp$) of a scatterer with respect to the beam axis is related to the axial positional change (s) of the scatterer by the tangent of the measurement angle or $s_\perp = s \cdot \tan(\theta)$. The perpendicular positional change at the center of the vessel is $0.5 \cdot \tan(45°)$ or 0.5 wavelength. The beamwidth normalized perpendicular positional change is $0.5/2 = 0.25$. This corresponds to a jitter of 3.7% (see Fig. 11). Hence, the midstream value of jitter for $\theta = 45°$ in Fig. 12(b) is largely a result of beamwidth modulation. The midstream values of jitter for the smaller vessels and larger angles are larger than the 3.7% baseline value for beamwidth modulation, indicating that the jitter introduced by velocity gradients is increasing.

The jitter from velocity gradients can be observed in Figs. 12(b)–(d) at the edges of the vessel where the effects of beamwidth modulation are minimal. For example, the beamwidth modulation of Fig. 12(b) is largest at midstream (since the scatterers are moving the fastest here) with a value of 3.7%. All other jitter above this baseline is a result of velocity gradients, and near the edges of the vessel the majority of the jitter is caused by the large velocity gradients.

In Figs. 12(c) and (d) the jitter is greater than the 3.7% baseline set by beamwidth modulation because the vessel diameters are smaller and have the same axial flow velocity and range cell size as the 24 wavelength diameter vessel in Fig. 12(b), hence, the velocity gradients must be greater.

Table I examines the interdependencies of window length, beamwidth, vessel diameter, and viewing angle.

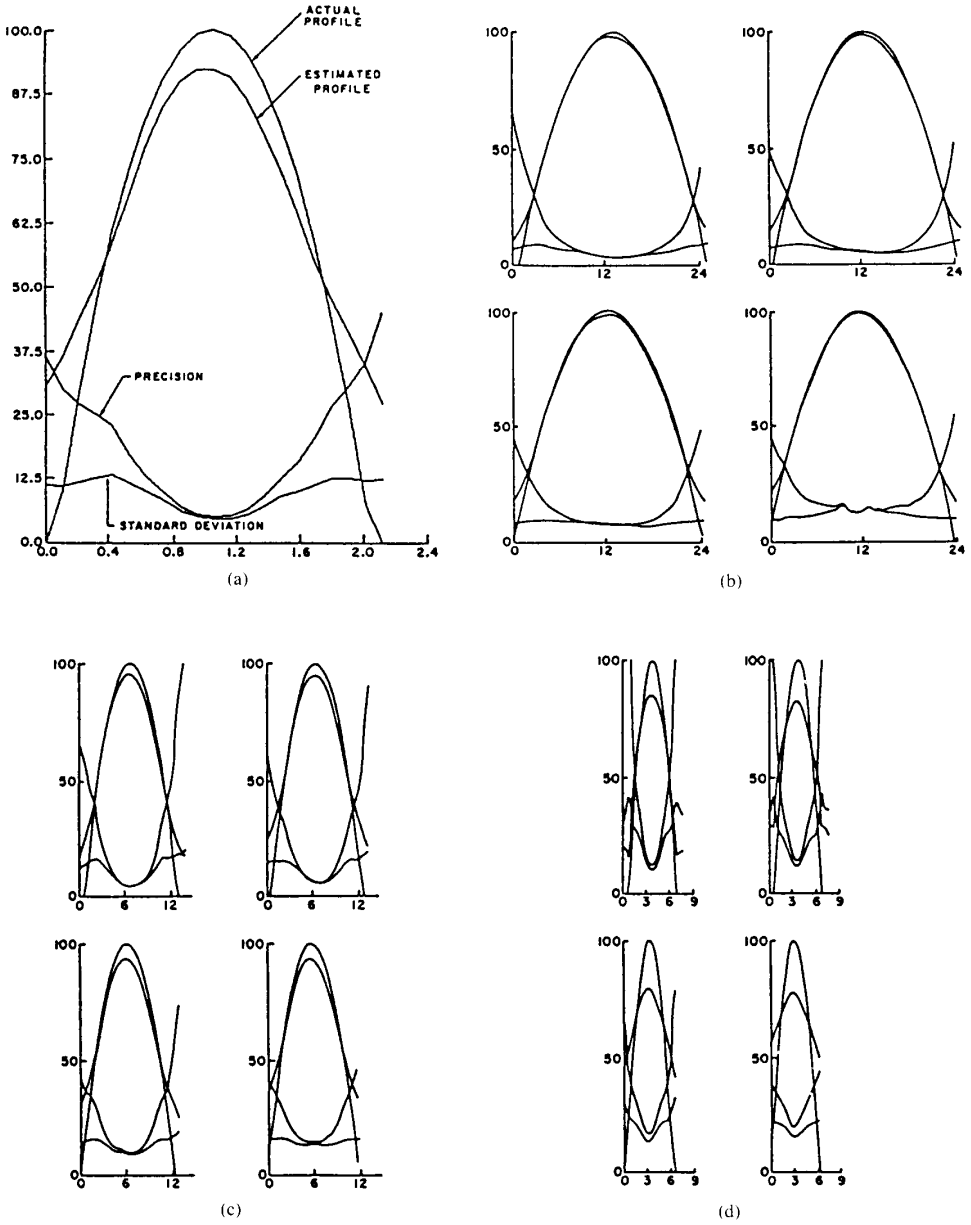

Fig. 12. (a) Graphic representation of parabolic velocity profiles of scatterers across vessel for computer simulation of time domain velocity extraction technique. This is format for (b), (c), and (d) in which the viewing angles are (upper left) 45°, (upper right) 55°, (lower left) 65° and (lower right) 75° and system Q is 4. Results of computer simulation of time-domain correlation method using the following parameters in wavelengths. (b) Vessel diameter of 24, maximum s of 0.5, transducer beamwidth of 2, and window length of 8. (c) Vessel diameter 12, maximum s of 0.5, transducer beamwidth of 2, and window length of 8. (d) Vessel diameter of 6, maximum s of 0.5, transducer beamwidth of 2, and a window length of 8.

The values of these quantities are approximately the same as the experimental quantities [14], [21], [26] and hence allow the results of the simulation to be compared with theory. Numbers without parentheses in Table I are the estimates of the actual flow at midstream divided by the actual flow at midstream multiplied by 100 (percentage bias) and the numbers in parentheses are the precisions of the velocity estimation (see (11)).

Increasing the viewing angle results in a decrease in the precision of the velocity estimation. This trend is followed for all combinations of the other three quantities except the 6-λ vessel with a BW = 4 for both window lengths. The reason for this exception is due to the estimate of the midstream flow is decreasing faster than the variance of the estimate. Hence, the precision (the ratio of the two aforementioned quantities) will increase. In-

TABLE I[a]

			Vessel Diameter (in wavelengths)		
			24	12	6
BW = 4	LEN = 4	θ = 45°	98.0(2.9)	93.1(6.6)	79.9(24.9)
"	"	θ = 55°	97.9(4.2)	92.6(7.6)	78.4(24.6)
"	"	θ = 65°	98.3(5.5)	93.0(8.4)	77.8(25.7)
"	"	θ = 75°	98.3(10.1)	93.2(12.7)	77.6(22.0)
"	LEN = 8	θ = 45°	97.6(2.2)	91.8(5.0)	76.8(23.9)
"	"	θ = 55°	97.6(2.9)	91.1(5.8)	73.9(22.2)
"	"	θ = 65°	97.6(4.1)	90.9(6.5)	70.8(21.3)
"	"	θ = 75°	97.5(7.2)	90.8(8.1)	69.6(20.0)
BW = 2	LEN = 4	θ = 45°	98.8(6.3)	97.0(7.0)	89.6(12.4)
"	"	θ = 55°	99.1(8.5)	96.4(8.6)	88.2(14.1)
"	"	θ = 65°	98.5(13.3)	96.1(14.1)	87.7(17.9)
"	"	θ = 75°	100.1(21.3)	95.3(22.9)	86.9(23.2)
"	LEN = 8	θ = 45°	98.6(3.7)	95.7(4.9)	85.2(12.1)
"	"	θ = 55°	98.4(5.1)	94.8(6.3)	81.9(14.6)
"	"	θ = 65°	98.1(8.3)	93.7(9.1)	80.0(16.4)
"	"	θ = 75°	99.2(13.6)	93.4(14.9)	77.4(19.8)

[a]Results of a computer simulation of the estimation of midstream flow (the number without parenthesis) and the precision in the velocity estimation (the number in parenthesis). The quantities varied are: the vessel diameter, the window length (LEN), the beamwidth of the transducer (BW), and the viewing angle (θ). The fixed quantities are velocity profile (parabolic), system $Q(4)$ and maximum axial separation ($s = 0.5\lambda$).

creasing the window length results in more precision as predicted in Fig. 7. Reducing the vessel diameter decreases the precision because the velocity gradients are higher in the smaller vessels for identical range cell sizes. A larger beamwidth has a greater precision in the larger tubes where the velocity gradients are small across the range cell. The smaller the window length the less bias there is in the velocity estimate. Bias is the deviation of the estimate from 100% at the vessel center flow. The shorter window length allows less local averaging of the velocity profile. The smaller the vessel diameter the greater the bias. Here the size of the range cell remained constant, but due to narrowing the velocity profile, the range cell must now contain a larger number of scatterers of differing velocities, hence, biasing the result downward. Bias gets worse for increasing viewing angle, especially for the smaller vessels. The larger angles reduce the axial contribution to the echo and increase the radial contribution (by the cosine of the viewing angle), hence, increasing the velocity gradients in the range cell (the range cell dimensions are independent of angle but dependent on beamwidth, window length, and impulse response). Large beamwidths have a greater bias. The beamwidth will smooth out velocity information, hence, detail in the range cell will be lost.

V. Conclusion

Some important observations can be drawn from the computer simulation results. The bias is directly related to the size of the range cell (a smaller range cell will average over a smaller portion of the velocity profile). Several quantities control the precision: 1) A narrower beamwidth will result in improved precision; 2) A longer window length will result in a better precision in the estimate of the actual shift; 3) A large velocity gradient across the range cell will result in poorer precision. Quantities 1) and 2) must be traded off against 3).

These results suggest an accurate one dimensional velocity profile across the vessel can be obtained. A high degree of precision between measured and true velocity exists over most of the vessel.

Acknowledgment

The authors acknowledge the useful comments from Robert W. Gill, Ilmar A. Hein, Robert Skidmore, Veijo Suorsa, Gregg E. Trahey, Peter N. T. Wells and the excellent reviewers are also very much appreciated.

References

[1] P. M. Embree and W. D. O'Brien, Jr., "Pulsed Doppler accuracy assessment due to frequency-dependent attenuation and Rayleigh scattering error sources," *IEEE Trans. Biomed. Eng.*, vol. 37, no. 3, pp. 322-326, Mar. 1990.

[2] R. W. Gill, "Measurement of blood flow by ultrasound: Accuracy and sources of error," *Ultrasound Med. Biol.*, vol. 11, pp. 625-641, 1985.

[3] C. P. Jethwa, M. Kaveh, G. R. Cooper, and F. Saggio, "Blood flow measurements using ultrasonic random signal Doppler system," *IEEE Trans. Sonics Ultrason.*, vol. SU-22, pp. 1-11, Jan. 1975.

[4] B. Angelsen, "Instantaneous frequency, mean frequency, and variance of mean frequency estimator for ultrasonic blood velocity Doppler signals," *IEEE Trans. Biomed. Eng.*, vol. BME-28, pp. 733-741, 1981.

[5] B. Angelsen and K. Kristoffersen, "Discrete time estimation of the mean Doppler frequency in ultrasonic blood velocity measurements," *IEEE Trans. Biomed. Engr.*, vol. BME-30, pp. 207-214, 1983.

[6] D. W. Baker, "Pulsed ultrasonic Doppler blood flow sensing," *IEEE Trans. Sonics Ultrason.*, vol. SU-17, pp. 170-185, 1970.

[7] P. A. Grandchamp, "A novel pulsed directional Doppler velocimeter, the phase-detection profilometer," in *Proc. 2nd Eur. Cong. Ultrasound in Med.*, pp. 137-143, 1975.

[8] M. Brandestini, "Application of the phase detection principle in a transcutaneous velocity profile meter," in *Proc. 2nd Eur. Cong. Ultrasound in Med.*, pp. 144-152, 1975.

[9] ——, "Topflow—A digital full-range Doppler velocity meter," *IEEE Trans. Sonics Ultrason.*, vol. SU-25, pp. 287-293, 1978.

[10] L. Hatle and B. Angelsen, *Doppler Ultrasound in Cardiology: Physical Principles and Clinical Application.* Philadelphia, PA: Lea and Febiger, 1982.

[11] P. Atkinson and J. P. Woodcock, *Doppler Ultrasound and Its Use in Clinical Measurement.* New York: Academic Press, 1982.

[12] C. Kasai, K. Namekawa, A. Koyano, and R. Omoto, "Real-time two-dimensional blood flow imaging using an autocorrelation technique," *IEEE Trans. Sonics Ultrason.*, vol. SU-32, pp. 458-464, 1985.

[13] M. I. Skolnik, *Radar Handbook.* New York: McGraw-Hill, 1970.

[14] P. M. Embree and W. D. O'Brien, Jr., "Volumetric blood flow *via* time domain correlation: Experimental verification," *IEEE Trans. Ultrason. Ferroelec. Freq. Contr.*, vol. 37, no. 3, pp. 176-189, May 1990.

[15] D. Dotti, E. Gatti, V. Svelto, A. Ugge, and P. Vidali, "Blood flow measurement by ultrasound correlation techniques," *Energia Nucleare*, vol. 23, pp. 571-575, Nov. 1976.

[16] M. Bassini, D. Dotti, E. Gatti, P. Pizzolati, and V. Svelto, "An ultrasonic non-invasive blood flowmeter based on cross-correlation techniques," *Ultrason. Int. Proc.*, 1979.

[17] M. Bassini, E. Gatti, T. Longo, G. Martinis, P. Pignoli, and P. Pizzolati, "*In vivo* recording of blood velocity profiles and studies *in vitro* of profile alterations induced by known stenoses," *Texas Heart Inst. J.*, vol. 9, pp. 185-194, June 1982.

[18] O. Bonnefous and P. Pesque, "Time domain formulation of pulse-Doppler ultrasound and blood velocity estimation by cross correlation," *Ultrason. Imaging*, vol. 8, pp. 75-85, 1986.

[19] O. Bonnefous, P. Pesque, and X. Bernard, "A new velocity estimator for color flow mapping," *IEEE Ultrason. Symp.*, 1986.
[20] B. Angelsen, "A theoretical study of the scattering from blood," *IEEE Trans. Biomed. Eng.*, vol. BME-27, pp. 61-67, 1980.
[21] P. M. Embree, "The accurate ultrasonic measurement of the volume flow of blood by time domain correlation," Ph.D. Thesis, Dept. Elec. Eng., University of Illinois, Urbana, IL, 1986.
[22] S. G. Foster, "A pulsed ultrasonic flowmeter employing time domain methods," Ph.D. Thesis in Dept. Elec. Eng., University of Illinois, Urbana, IL, 1984.
[23] R. E. Boucher and J. C. Hassab, "Analysis of discrete implementation of generalized cross correlator," *IEEE Trans. Acoust., Speech Signal Processing*, vol. ASSP-29, pp. 609-611, 1981.
[24] C. W. Helstrom, *Statistical Theory of Signal Detection.* Oxford, UK: Pergamon, 1960.
[25] P. M. Woodward, *Probability and Information Theory, With Application to Radar.* Oxford, UK: Pergamon, 1953.

Steven G. Foster, photograph and biography not available at time of publication.

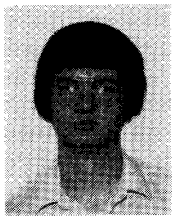

Paul M. Embree (S'80-M'81-S'81-M'82-S'83-M'85) was born in Reading, PA in 1959. He received the B.S. degree in electrical engineering from Lehigh University, Bethlehem, PA, in 1981, and the M.S. and Ph.D. degrees in electrical engineering from University of Illinois, Urbana, IL, in 1982 and 1986, respectively.

From 1981 to 1982 he was a member of technical staff at Bell Telephone Laboratories, Reading, PA, where he worked in the field of analog filter design of CMOS integrated circuits. After completing the Ph.D. in the field of medical ultrasound, he joined Philips Ultrasound, Santa Ana, CA, in 1986. His current interests involve the analysis and design of real-time signal processing systems for special purpose high speed applications. Embedded programmable signal processors for real-time DSP applications are of particular interest. He has published several papers in the area of medical ultrasound and recently authored the book *C Language Algorithms for Digital Signal Processing*.

He is a member of SPIE, the IEEE Acoustics, Speech and Signal Processing Society and the IEEE Ultrasonics, Ferroelectrics, and Frequency Control Society.

William D. O'Brien, Jr. (S'64-M'70-SM'79-F'89) was born in Chicago, IL, on July 19, 1942. He received the B.S., M.S., and Ph.D. degrees from the University of Illinois, Urbana, in 1966, 1968, and 1970, respectively.

From 1971-1975 he was with the Bureau of Radiological Health (currently the Center for Devices and Radiological Health) of the U.S. Food and Drug Administration. Since 1975 he has been at the University of Illinois where he is a Professor of Electrical and Computer Engineering and of Bioengineering, College of Engineering, and Professor of Bioengineering, College of Medicine. His research interests involve the many areas of ultrasound-tissue interaction, including spectroscopy, risk assessment, biological effects, tissue characterization, dosimetry, blood flow measurements, and acoustic microscopy, for which he has published more than 90 papers.

Dr. O'Brien is Editor-in-Chief of the IEEE TRANSACTIONS ON ULTRASONICS, FERROELECTRICS, AND FREQUENCY CONTROL. He is a Fellow of IEEE, the Acoustical Society of America and the American Institute of Ultrasound in Medicine (AIUM) and was the recipient of an IEEE Centennial Medal (1984) and the AIUM Presidential Recognition Award (1985). He was President (1982-1983) of the IEEE Sonics and Ultrasonics Group (currently the IEEE Ultrasonics, Ferroelectrics, and Frequency Control Society), Co-Chairman of the 1981 IEEE Ultrasonics Symposium and General Chairman of the 1988 IEEE Ultrasonics Symposium. He is currently AIUM's President (1988-1991). He is on the Editorial Boards of the *Journal of Ultrasound in Medicine*, *Journal of Cardiovascular Technology*, and *Journal of Diagnostic Medical Sonography*.